Title: Hypoxia-inducible factor 1 signaling drives placental aging and can elicit inflammatory changes in uterine myocytes

Authors: Erin J. Ciampa[1], Padraich Flahardy[1], Harini Srinivasan[2], Christopher Jacobs[2], Linus Tsai[2], S. Ananth Karumanchi[3], Samir M. Parikh[4]

Affiliations:

[1] Department of Anesthesia, Critical Care, and Pain Medicine, Beth Israel Deaconess Medical Center, Harvard Medical School, Boston MA, USA

[2] Division of Endocrinology, Beth Israel Deaconess Medical Center, Harvard Medical School, Boston MA, USA

[3] Department of Medicine, Cedars-Sinai Medical Center, Los Angeles CA, USA

[4] Division of Nephrology, Departments of Medicine and Pharmacology, University of Texas Southwestern Medical School, Dallas TX, USA

Address correspondence to: Erin Ciampa, MD PhD. Beth Israel Deaconess Medical Center, Department of Anesthesia, Critical Care, and Pain Medicine. 330 Brookline Avenue, FD-407, Boston MA 02215. Email: eciampa@bidmc.harvard.edu

Abstract:

Most cases of pre-term labor have unknown cause, and the burden of preterm birth on neonatal and child health is immense. Placental aging has been proposed to promote labor onset, but specific mechanisms remain elusive. We report here findings stemming from an unbiased transcriptomic analysis of healthy mouse placenta, which revealed that hypoxia-inducible factor 1 (HIF-1) stabilization is a hallmark of advanced gestational timepoints, accompanied by mitochondrial dysfunction and cellular senescence. We validated these gestational age-associated changes through similar findings in human placenta. In parallel in primary mouse trophoblasts and human choriocarcinoma JAR cells, we modeled HIF-1 induction using prolyl hydroxylase inhibitors cobalt chloride ($CoCl_2$) and dimethyloxalylglycine (DMOG), and demonstrated that mitochondrial dysfunction and cellular senescence occur secondary to HIF-1 stabilization. Whole transcriptome analysis revealed that HIF-1 stabilization in JAR cells recapitulated the dysregulation of several pathways observed in aged placenta. Further, conditioned media from cultured trophoblasts following HIF-1 induction is sufficient to induce a contractile phenotype in immortalized uterine myocytes, suggesting a mechanism by which the aging placenta may help drive the transition from uterine quiescence to contractility at the onset of labor. These results provide clear evidence for placental aging in normal pregnancy. Mechanistic dissection of this phenomenon further demonstrates how hypoxia in late gestation may be both a causal determinant of the mitochondrial dysfunction and senescence observed within the trophoblast as well as a trigger to induce uterine contraction.

Main:

Preterm birth (birth prior to 37 completed weeks of gestation) is a massive global health burden: it leads all causes of death in neonates and children to the age of 5 worldwide(1), and survivors face a broad array of short- and long-term health challenges(2). Most preterm births in the United States are due to spontaneous onset of preterm labor, with unknown underlying cause(3). Preterm labor has proven difficult to treat; there currently exist no highly effective interventions that prevent spontaneous preterm birth (SPTB)(4). The dearth of effective

treatments stems from our lack of understanding about the mechanisms responsible for spontaneous onset of labor, both preterm and at term.

The placenta defines the maternal-fetal interface; it is capable of profoundly influencing both maternal and fetal physiology(5-7), and it is subject to remodeling in response to its local environment(8). Placental disease is known to contribute to other disorders of pregnancy including preeclampsia(9-11) and intrauterine growth restriction(12, 13) and there is increasing interest in its potential role as a driver of preterm labor(14-16).

Recent studies have found that placentas from pregnancies that resulted in SPTB have unique metabolomic and transcriptomic signatures from term counterparts(17-19), broadly implicating the stress response, inflammation, and various metabolic pathways. It has been challenging to narrow these findings or translate them for mechanistic relevance, given the lack of suitable culture systems that integrate experimental manipulation of placental cells with the uterine myocyte response. Furthermore, interpretation of profiling studies centered on human placentas from SPTB is sharply limited by the lack of gestational age-matched controls, making it difficult to untangle the effects of gestational age from factors driving premature labor. The placenta encounters a dynamic local environment across its lifetime and faces evolving needs of the growing fetus, so the context of normal gestational age-related changes is vital for the correct interpretation of molecular characteristics distinguishing a SPTB placenta. Defining the molecular-level changes in the *healthy* placenta across gestation, and their potential effects on the timing of labor onset would therefore address important knowledge gaps.

Here we report findings from unbiased transcriptomic analysis of healthy mouse placenta, which highlighted hypoxia-inducible factor 1 (HIF-1) signaling as a hallmark of advanced gestational timepoints, accompanied by mitochondrial dysfunction and cellular senescence. We validated these findings in human placenta, then modeled HIF-1 induction with two different stimuli and in two trophoblast cell models, demonstrating that mitochondrial dysfunction and cellular senescence arise secondary to HIF-1 stabilization. Whole transcriptome analysis

revealed that upon HIF-1 stabilization, a trophoblast cell line acquires signatures that recapitulate the aged placenta. Finally, we show that conditioned media from these cells is sufficient to potentiate a contractile phenotype in uterine myocytes, implicating a mechanism by which the aging placenta may help drive the transition from uterine quiescence to contractility at the onset of labor.

Results

To illuminate gestational age-dependent transcriptional changes in across a healthy pregnancy, we collected whole mouse placentas at 48h intervals spanning embryonic day 13.5 to 17.5 (e13.5-e17.5) and quantified mRNA and protein targets that emerged from network analysis of an independently published microarray dataset from healthy mouse pregnancies. Upon searching Gene Expression Omnibus (GEO) datasets for "placenta AND transcriptome", we were surprised that among 326 results, only nine included data from normal placenta across a series of gestational timepoints extending to late pregnancy (20-26) (**Figure 1A**). We applied weighted gene correlation network analysis (WGCNA) to a microarray study of mouse placenta (20) spanning e8.5 to postnatal day 0 (p0) to assess the mRNA signature of the aging mouse placenta, using the dataset with the best temporal resolution across gestation. Distinct clusters emerged, each reflecting a group of genes whose expression changes across timepoints in a unified way (**Figure 1B**). Genes in the 'blue' cluster (2,444 genes) showed increasingly positive correlation with advancing gestational timepoints; KEGG functional pathways significantly overrepresented among these genes include HIF1 signaling, AMPK signaling, and cellular senescence. Genes in the 'turquoise' cluster (4,022 genes) showed increasingly negative correlation to advancing timepoints; KEGG functional pathways significantly overrepresented among these genes include the citric acid cycle, mitochondrial complex I biogenesis, and the mitotic cell cycle.

To validate the dynamic pathway activity suggested by the WGCNA, we quantified mRNA expression of the senescence marker *Glb1* in our mouse placentas, which mirrored the WGCNA finding that cellular senescence in the placenta peaks in the final days of gestation (**Figure 1C**;

p=0.02). HIF-1 protein abundance was found to peak at e17.5 (**Figure 1D**, p=0.02) and HIF-1 targets *Hk2* and *Glut1* likewise confirmed increasing HIF-1 activation with advancing gestational age through e17.5 (**Figure 1E**; p< 0.0001). Of note, a modest but significant fetal sex-dependent difference in HIF-1 target expression (but not *Glb1*) was also observed across timepoints (**Supplemental Figure 1A-B**). To assess changes in mitochondrial abundance across gestation, we measured COX IV protein expression and found it declined progressively across murine gestation (**Figure 1F**; p=0.006) as predicted by the WGCNA.

Having observed a pattern of declining mitochondrial abundance in the placenta with advancing gestational age, we next investigated the mitochondrial DNA (mtDNA) lesion rate. The mitochondrial genome is particularly vulnerable to reactive oxygen species (ROS) insults, and mtDNA damage participates in a vicious cycle with mitochondrial dysfunction and further ROS production; these effects are observed in a number of age-related diseases in various tissues(27) and may drive age-associated loss of function(28). We employed a semi-long run real-time qPCR approach(29) to quantify relative mtDNA lesion rates in mouse placentas, normalized to e13.5. There was a measurable increase in the mtDNA lesion rate in the D-loop and COII/ATPase 6 regions of the mitochondrial genome at e17.5 (**Figure 1G**). Together, these results reflect a series of coordinated changes as gestation progresses —namely HIF-1 signaling induction, decreasing mitochondrial abundance, accumulating ROS stress, and escalating cellular senescence — confirming patterns we discovered through reanalysis of published transcriptomic data.

We next probed human placentas for changes in cellular senescence, HIF-1 signaling and mitochondrial abundance with increasing gestational age. Studying normal human placenta at a range of gestational ages beyond the second trimester is challenging, as placental sampling is usually only possible after delivery, and most deliveries associated with healthy pregnancies occur at term. We therefore sought to capitalize on rare exceptions such as cases of placenta previa, vasa previa, or uterine dehiscence. With an objective to compare term versus preterm placentas, yet minimize confounding factors that accompany labor and disease states that

could be expected to affect placental health, we designed a case-control study using the following exclusion criteria: onset of labor prior to delivery (spontaneous or induced); maternal history of hypertension, asthma, diabetes, or autoimmune disease; pregnancy complicated by gestational hypertension, gestational diabetes, preeclampsia, multiples, fetal anomalies, placenta accreta spectrum disorder, or smoking during pregnancy. Placentas from 8 cesarean deliveries occurring before 35 weeks gestation and 10 cesarean deliveries occurring after 39 weeks gestation were studied (mean gestational age 34.2 +/- 0.92 weeks versus 39.6 +/- 0.3, $p<0.0001$, **Table 1**). Maternal characteristics including race, nulliparity, and obesity were not statistically different across the early versus late groups; there was a modest but statistically significant difference in maternal age at the time of delivery (32.5 +/- 1.8 years versus 36.5 +/- 3.1 for early gestation versus late, $p = 0.006$). The distribution of fetal sex was not different among groups ($p=0.18$).

We found increased expression of the cellular senescence marker *GLB1* in the higher-gestational age samples ($p=0.07$, **Figure 2A**), consistent with the gestational age-dependent trend seen in mouse placenta. The relative abundance of HIF-1 targets *HK-2* and *GLUT1* (**Figure 2B**, $p=0.09$) each trended higher among later-gestational age samples, suggesting that HIF-1 signaling increases with gestational age in normal human pregnancies as we found in mice. We also examined mitochondrial abundance in the two groups and found that mitochondrial RNA transcripts *ATP6* and *COX2* were significantly decreased (**Figure 2C**, $p=0.008$) and COX IV protein abundance was lower at the later timepoint (**Figure 2D**, $p=0.09$).

Having established that cellular senescence, HIF-1 signaling, and mitochondrial dysregulation each occur with advancing gestational age in both mouse and human placentas, we hypothesized that HIF-1 induction could be upstream of mitochondrial dysregulation and cellular senescence, as suggested by emerging aging research(30-32). To test this hypothesis, we established a pharmacological model of HIF-1 induction in primary mouse trophoblasts using cobalt chloride, a prolyl hydroxylase inhibitor that stabilizes HIF-1α and has been widely used to model hypoxia. After six hours of $CoCl_2$ exposure, we confirmed HIF-1 protein

accumulation in cultured trophoblasts (**Figure 3A**). After 48 hours of $CoCl_2$ exposure, mouse trophoblasts exhibit decreased mitochondrial abundance, by *Cox2* expression (**Figure 3B**), Cox IV protein abundance (**Figure 3C**) and an increase in senescence-associated beta galactosidase (SA-βGal), encoded by *Glb1* (**Figure 3D**) and detected as a blue stain in an X-gal assay for senescence (**Figure 3E**). These findings suggest that HIF-1 stabilization induces subsequent mitochondrial dysfunction and senescence.

Primary trophoblasts undergo spontaneous syncytialization in culture, a change that limits both the duration of study and may also confound the interpretation of change in key metabolic regulators(33). We therefore also modeled HIF-1 activation in JAR cells, a trophoblast cell line that does not undergo syncytialization(34). Consistent with our results in primary cells, we found that (a) HIF-1 is stabilized in $CoCl_2$ treated JAR cells (**Figure 4A**); and (b) that after 6 days of exposure, mitochondrial DNA and protein abundance declined in JAR cells (**Figure 4B-C**). We further defined the time course of mitochondrial dysregulation. At 48 hours after $CoCl_2$ administration we found no measurable decline in mitochondrial abundance, but by 72 hours the effect begins to appear (**Supplementary Figure 2A**). Furthermore, after 6 days of $CoCl_2$ exposure, mitochondrial polarization is impaired (**Figure 4D**), and mitochondrial reactive oxygen species accumulate (**Figure 4E**). Finally, we observed pronounced signs of cellular senescence: morphological hallmarks (cellular swelling) and β-galactosidase overexpression (**Figure 4F**); growth arrest which persists for days after removal of the HIF-1 stabilizing compound (**Figure 4G**); and a senescence-associated secretory phenotype (SASP, **Figure 4H**) reflected by increases in expression of VEGF, TNFα and IL-1α and a decrease in the anti-inflammatory cytokine IL-10.

We conducted additional studies to confirm that cell death was not a primary contributor to the lack of proliferation. Propidium iodide staining with quantitative fluorescence cytometry indicated that $CoCl_2$ treatment only increased cell death by 0-3% (**Supplementary Figure 2B**). Importantly, cells remained adherent and continued to acidify culture medium beyond 14 days with $CoCl_2$ exposure, providing confidence that HIF-1 stabilization induces a phenotype

characterized by predominantly viable cells that are no longer proliferating, namely cellular senescence. Finally, to assess whether the effects we observed were attributable to HIF-1 stabilization and not an off-target effect of $CoCl_2$, we also evaluated an alternative prolyl hydroxylase inhibitor, DMOG, and found similar effects on HIF-1, mitochondrial abundance and cellular senescence (**Supplementary Figure 2C-E**).

To determine if other features of the aged placenta phenotype were recapitulated in this model, we performed whole transcriptome analysis via RNA-Seq. Differential expression ($\log_2$ fold change > 1; FDR < 0.05) was found for 2188 upregulated and 1389 downregulated genes (**Figure 4I**). Gene set enrichment analysis revealed that chemical hypoxia led to upregulation of inflammatory signaling; and downregulation of the TCA cycle, mitochondrial biogenesis, and respiratory electron transport. These data therefore recapitulated metabolic patterns that emerged from time course transcriptomic analysis of intact placentas (**Figure 1**).

The onset of labor is accompanied by a transformation of the uterus from quiescence into a distinct physiologic state in which it can generate powerful, coordinated contractions. This phenotypic change is characterized by upregulation of a cadre of contraction associated proteins (CAPs), notably: IL-6, cyclooxygenase-2 (COX-2, encoded by *PTGS2*; key inducible enzyme in prostaglandin synthesis pathway), prostaglandin F2-a receptor (encoded by FP), IL-6, and connexin 43 (Cx43, encoded by *GJA1*; gap junction protein with critical role in intercellular communication during labor (35)). Phenotypic switching can be modeled in primary and immortalized uterine myocytes upon stimulation with inflammatory mediators such as IL1β, PGF2α, and thrombin (36-38).

To test whether primary placental metabolic disruptions could crosstalk with uterine myocytes to trigger the contractile phenotype, we collected conditioned media from our JAR cell model of HIF-1-driven senescence and measured the effect on expression of CAPs in uterine myocytes (hTERT-HM cells). To our surprise, we observed a robust and specific effect: stimulation of uterine myocytes with conditioned media from JAR cells treated with $CoCl_2$ (but not from

untreated JAR cells) recapitulated the induction of *PTGS2*, *GJA1*, *FP*, and *IL-6* expression seen with IL-1β stimulation; moreover, costimulation with conditioned media from hypoxic JAR cells potentiated the IL-1β effect (**Figure 5A-D**).

Discussion

The subject of whether the healthy placenta undergoes aging (with accompanying dysfunction) within its 40-week lifespan has been of great interest and debate for many years. Age-related functional decline is a near-universal phenomenon affecting many tissues, but the underlying biochemical driving factors vary widely depending on the context of cell type and local stressors. Mechanisms well described in other tissues are rooted in genomic instability, mitochondrial dysfunction and oxidative stress, nutrient deprivation and metabolic insufficiency, or loss of proteostasis(39). While characterization of the placenta as an aging organ appeared in the literature beginning nearly fifty years ago(40, 41), a counter-argument has been offered that there is no logical reason for the placenta to undergo accelerated aging relative to the fetus, since both share the same genes and environment(42). A third viewpoint proposes that aging in the placenta is indicative of a disease state—not normal progression of healthy gestation—one usually reflective of maladaptive responses to oxidative stress (43-47). Finally, recent reports have noted prominent signs of aging in another fetally derived tissue, the chorioamniotic membranes, in healthy pregnancies(48), and have linked aging of the fetal membranes to the onset of labor(49, 50). The results presented here span mouse and human placentas to provide clear evidence for placental aging in normal pregnancy. Mechanistic dissection of this phenomenon further demonstrates how hypoxia in late gestation may be both a causal determinant of the mitochondrial dysfunction and senescence observed within the trophoblast as well as a trigger to induce uterine contraction.

To our knowledge, this is the first report to propose that placental aging in healthy pregnancy is characterized by induction of HIF-1 signaling, accompanied by downstream effects including mitochondrial dysfunction and cellular senescence. These findings have implications for the role

of the placenta in signaling that promotes the onset of labor, particularly given our demonstration that upon HIF-1 stabilization, trophoblasts can induce inflammatory changes in uterine myocytes, recapitulating critical components of the contractile phenotype adopted by myocytes during labor. Important next steps prompted by this work include determining the specific components of the secretome of HIF-1-activated trophoblasts which are responsible for inducing myocyte transformation. Additionally, having established that HIF-1 signaling and mitochondrial dysfunction are upstream of cellular senescence in trophoblasts in late gestation in normal pregnancies, future studies can investigate whether factors that modulate this pathway could increase or decrease vulnerability to preterm labor.

Our results suggest that HIF-1 becomes stabilized late in gestation, and this could be secondary to the onset of hypoxia sensing as oxygen demand outstrips supply in the fetoplacental unit. However, placental hypoxia has been difficult to examine *in vivo*. Despite evolving approaches for measurement of placental oxygenation, findings have varied widely and adequate spatiotemporal resolution has so far been challenging (51). However, it is apparent that due to arteriovenous shunting and high metabolic extraction rates, the placenta experiences hypoxia throughout pregnancy with a reported partial pressure of oxygen 30-50 mm Hg in the intervillous space, so perhaps a relevant question is what *prevents* HIF-1 stabilization and its downstream effects early in gestation. It is possible that the gestational-age-dependent HIF-1 induction we observed reflects not a change in oxygen availability, but rather a change in other HIF regulatory factors such as nicotinamide adenine dinucleotide (NAD^+) depletion, as has been demonstrated to occur in muscle and is accompanied by metabolic reprogramming and mitochondrial decline (52). Importantly, replenishment of NAD^+ was shown to restore markers of mitochondrial function in these aged cells, suggesting that mitochondrial effects of HIF-1-driven aging are reversible in some systems. Separately, a recent study which compared the miR-nomes of 1st- versus 3rd-trimester human placenta highlighted differential expression of miRNAs with functional links to silencing of hypoxia response and cellular senescence pathways in the first trimester(53). Future investigations into the impact of placental HIF-1 regulation will

require a more precise understanding of placental oxygenation *in vivo* and a sophisticated approach to model these factors in placental explants or other cellular systems.

The shift in metabolic phenotype away from oxidative respiration in late pregnancy as demonstrated by our transcriptomics analysis is consistent with earlier findings from respirometry studies in mouse placenta (54), where rates of oxidative phosphorylation were noted to decline from e14 to e19, particularly in the labyrinthine zone. It is still unclear if this shift reflects changing substrate availability, or oxygen content, or perhaps the metabolic needs of the developing fetus. A better understanding of the dynamic metabolism of the placenta across gestation will be crucial for developing strategies for optimizing placental health, with major implications for both maternal and fetal outcomes. For example, placental metabolomics studies with a gestational time series could help corroborate the metabolic implications interpreted from our transcriptomic data, while single-cell transcriptomics across advancing gestational age in healthy placentas would offer critical cell-type localization of specific metabolic events noted to occur late in pregnancy. Future studies aimed at targeted manipulation of placental metabolism *in vivo*, whether pharmacologically or genetically, are needed to define the physiologic relevance of these findings.

Our data have implications for other adverse pregnancy outcomes beyond preterm birth, including intrauterine growth restriction and preeclampsia. There is evidence that these conditions have overlapping pathophysiologic mechanisms(55-59) and each has been tied to abnormal aging of the placenta(43). A thread unifying aging and each of these diseases is the impact of accumulating oxidative stress, whether due to increased ROS production or weakened antioxidant defenses. In our model of HIF-1 activation we observed substantial ROS accumulation, therefore future studies could examine whether dysregulation of HIF-1 signaling contributes to these disease states as well.

In summary, we report a molecular characterization of placental aging phenomena occurring in normal pregnancies, stemming from induction of HIF-1 signaling and downstream

mitochondrial dysfunction and cellular senescence. These findings establish aging in the placenta as a feature of normal gestation; identify HIF-1 signaling as an upstream trigger leading to mitochondrial dysfunction and senescence in the placenta; and propose that the secretome of senescent trophoblasts is sufficient to trigger uterine myocyte transformation. These findings may have important implications for illuminating the factors that determine gestational length both in health and disease.

Figure Legends:

Figure 1. Placental aging is characterized by cellular senescence, HIF-1 signaling, and mitochondrial dysregulation in mouse. 326 GEO datasets were identified by the search terms "placenta" and "transcriptome"; nine met criteria for containing placental transcriptomic data reflecting normal physiology across multiple timepoints spanning into the final 1/3 of pregnancy (A). Dataset used for analysis in B indicated in yellow. Functional pathways overrepresented in gene clusters found to increase (blue) and decrease (turquoise) across gestation highlight enhanced cellular senescence, increased HIF-1 signaling, and decreased mitochondrial synthesis and respiration late in pregnancy (B). Whole-placenta expression of senescence marker *Glb1* peaks at e17.5 (C; one-way ANOVA p=0.0048). Hif-1 protein abundance is higher at e17.5 versus e13.5 and e15.5 (D; one-way ANOVA p=0.019), as is expression of Hif-1 targets *Hk2* and *Glut1* (E; two-way ANOVA p<0.0001 for gestational age factor). Mitochondrial abundance, reflected by COX IV protein expression, decreases with advancing gestational age (F, one-way ANOVA p=0.0064), and mitochondrial DNA lesion rate peaks at e17.5 in the genomic regions of the D-loop (one-way ANOVA p=0.0001), COII/ATPase6 (p=0.0027), and ND5 (p=0.036) (G).

Figure 2. Senescence, HIF-1 signaling, and decreased mitochondrial abundance characterize late-gestation human placenta. Expression of senescence marker GLB1 is increased placentas from > 39 week cohort (A; p=0.067), as are HIF-1 targets HK-2 and GLUT1 (B; two-way ANOVA gestational age factor p=0.09). Mitochondrial abundance, reflected by mitochondrial genes

ATP6 and COX2 (C; two-way ANOVA gestational age factor p=0.008) and COX IV protein (D; p=0.087) decreases with advancing gestational age.

Figure 3. Short-term HIF-1 stabilization in primary mouse trophoblasts leads to decreased mitochondrial abundance and cellular senescence. HIF-1 is detected in cultured trophoblasts exposed to $CoCl_2$ (A). After 48 hours of CoCl2 exposure, trophoblasts exhibit decreased mitochondrial abundance reflected by *Cox2* (B; p=0.014) and COX IV (C; p=0.0047) expression levels. Senescence marker Glb1 is increased (D; p=0.0384) and SA-βGal accumulation is noted by X-gal assay (E; p=0.0115).

Figure 4. Long-term HIF-1 stabilization in JAR cells leads to mitochondrial dysfunction, cellular senescence, and metabolic reprogramming. $CoCl_2$ exposure to cultured JAR cells stabilizes HIF-1 (A). After 6 days of $CoCl_2$ exposure, mitochondrial abundance is decreased as reflected by a drop in the mitochondrial:nuclear DNA copy number (B; p=0.0022) and a decrease in COX IV protein (C; p<0.0001). Cells also exhibit augmented signs of mitochondrial dysfunction after 6d of CoCl2, including TMRE (D; two-way ANOVA $CoCl_2$ factor p<0.0001) and MitoSox staining (E; p=0.0003). SA-βGal staining reflects a high proportion of senescent cells (F; p<0.0001) and growth arrest is confirmed by cell counting following a 6-day pre-treatment with $CoCl_2$ (G; two-way ANOVA p<0.0001 for interaction of $CoCl_2$ factor with time). SASP candidates VEGF, TNFa, IL-1a, and IL10 are dysregulated after $CoCl_2$ exposure (H; *, adjusted p<0.00001). RNA Seq revealed upregulation of 2188 and downregulation of 1389 genes (I; genes with $|\log_2(FC)| > 1$ and -log(FDR)>2 indicated in red) after CoCl2 treatment, with geneset enrichment analysis revealing several pathways significantly dysregulated after $CoCl_2$ treatment recapitulating changes seen in transcriptomic analysis of late versus early gestation mouse placenta.

Figure 5. Conditioned media from JAR cells following HIF-1 stabilization induces expression of contractile-associated proteins in immortalized human uterine myocytes. hTERT-HM expression of *PTGS2* (A), *GJA1* (B), *FP* (C), and *IL6* (D) was induced by conditioned media from JAR cells (JAR) following $CoCl_2$ treatment (but not in control conditions), similar to (and

potentiating) the effect of stimulation of myocytes by exogenous IL-1β. *, $p<0.01$ versus no additive (blue bar). Ns, no significant difference versus no additive.

Data Availability:

Full datasets (WGCNA and RNA Seq) will be made available at the time of publication.

Methods:

Mouse protocols. All animal experiments are approved by the Beth Israel Deaconess Medical Center Institutional Animal Care and Use Committee.

Timed placenta collection: C57BL/6 mice were fed a chow diet and housed at 20°C in a 12-hour light/12-hour dark cycle. Nulliparous females (< 6 months of age) were housed for a single dark cycle (midnight = gestational day 0) with a stud male. On gestational day e13.5-17.5, placentas were isolated via laparotomy from pregnant females anesthetized via surgical-plane isoflurane. Placentas were quartered, immersion-rinsed in dH_2O and blotted dry, then snap frozen in liquid nitrogen and stored at -80°C prior to use.

Mouse trophoblast isolation: Protocol described in full in Pennington *et al*(60). On gestational day e15.5, placentas were collected via laparotomy from pregnant females anesthetized with surgical-plane isoflurane. After dissection, placentas were quartered, immersion-rinsed in dH2O, then placed in ice-cold digestion buffer: DMEM plus HEPES 20 mM, collagenase 1mg/mL, and DNase I 4000U/mL. Placentas were digested for 20-40 minutes at 37°C with trituration and examined under a microscope until optimal digestion achieved. Digested cells were passed through a 70 micron strainer, washed in DMEM, then separated using a Percoll gradient. Trophoblast fraction was washed once more then plated in complete medium: DMEM with HEPES 20 mM, FBS 10%, and supplemented with sodium pyruvate, pen-strep-glutamine, non-essential amino acids, and gentamicin.

Human placental specimens.

Human placental specimens and data were biobanked and accessed under protocols approved by the Beth Israel Deaconess Medical Center Institutional Review Board. Placenta samples were collected at the time of cesarean delivery, within 20 minutes of delivery of the placenta. Placental tissue was sampled from approximately 1cm deep to the maternal surface after dissecting away membranes. Cotyledons from all 4 quadrants were collected and minced

together prior to immersion rinse in dH2O and storage of separate aliquots by snap freezing versus immersion in RNA Later. All samples were stored at -80°C prior to use.

Cell culture.

JAR choriocarcinoma cells (ATCC) were grown in RPMI1640 media (4.5 g/L glucose) with 10% FBS. Adherent JAR cells were treated with HIF1-stabilizing agents dissolved in 1X PBS (pH 7.4): cobalt chloride hexahydrate (100 µM $CoCl_2$, Millipore Sigma) and dimethyloxalylglycine, N-(methoxyoxoacetyl)-glycine methyl ester (1 mM DMOG, Millipore Sigma). JAR cells were treated with 100 µM $CoCl_2$ or 1 mM DMOG in culture media as indicated prior to endpoint assays.

Preparation of conditioned media: On day 5 of JAR cell treatment with $CoCl_2$ (versus control condition), media exchange was performed to apply serum-free media for both conditions. 24 hours later, conditioned media samples were collected and applied to 10 kDa molecular weight cutoff filters (Amicon Ultra), with centrifugation for 20 minutes at 4000 x *g*, 4°C. Filters were washed with one volume of hTERT-HM base medium (see below), with repeat centrifugation. Concentrated proteins retained in suspension above the filter were collected and stored at -80°C.

hTERT-HM cells (generously supplied by Dr. Jennifer Condon, Wayne State) were grown in DMEM/F12 medium (Gibco) with 10% FBS and Antibiotic-Antimycotic (1X, Gibco). Cells were stimulated by addition of recombinant human IL-1β (R&D Systems) and/or filter-concentrated JAR cell conditioned media as indicated, 6 hours prior to collection of cellular RNA.

RT – qPCR. Total RNA was reverse transcribed to cDNA with the Superscript III reverse transcriptase (Invitrogen) system with random hexamer primers (Invitrogen) according to manufacturer's instructions. cDNA was amplified via real-time quantitative PCR with TaqMan Fast Advanced Master Mix (Applied Biosystems) or SYBR Green PCR Master mix (Qiagen) in a QuantStudio 6 Flex Real-Time PCR System (Applied Biosystems). In mouse samples, target gene expression was normalized to endogenous levels of housekeeping gene, β-actin. In human samples, target gene expression was normalized to endogenous levels of housekeeping gene, YWHAZ (TaqMan) or β-actin (SYBR). Mouse and human primers are listed in Supplemental Table 1.

mtDNA damage assay. Mitochondrial DNA damage was assayed from total DNA via a semi-long run real-time PCR approach, as described elsewhere(29). Briefly, separate qPCR reactions were assayed to compare a long versus short amplicon representing each genomic region. A lesion rate per 10 kb of mtDNA was calculated as: lesion rate $= \frac{10000\ (bp)}{size\ of\ long\ fragment\ (bp)} * (1 - FC_{long-short})$, with $FC_{long-short} = 2^{-\Delta\Delta Ct}$ calculated in the usual method. Primers are listed in Supplementary Table 1.

Relative mtDNA copy number. qPCR assays for nuclear and mitochondrial genes were performed using total DNA as a template. Relative mitochondrial DNA was calculated as: follows: mt:nuc DNA copy number $= 2 * 2^{\Delta Ct}$, where $\Delta Ct = Ct_{nuclear\ gene} - Ct_{mitochondrial\ gene}$. Primers are listed in Supplementary Table 1.

Supplementary Table 1. Primers

Mouse

Target	Sequence	Platform
GLB1	Mm00515342_m1	TaqMan
HK-2	Mm00443385_m1	TaqMan
GLUT1	Mm00441473_m1	TaqMan
D loop (long, 801 bp amplicon)	F: CGTACATTAAACTATTTTCCCCAAG R: GAGTTTTGGTTCACGGAACAT	SYBR
COII/ATPase 6 (long, 855 bp amplicon)	F: TTGGTCTACAAGACGCCACA R: ATTTTGGTGAAGGTGCCAGT	SYBR
ND5 (long, 930 bp amplicon)	F: CGCCTACTCCTCAGTTAGCC R: ATGGTGACTCAGTGCCAGGT	SYBR
ND2/ND1 (long, 832 bp amplicon)	F: GGATGAGCCTCAAACTCCAA R: ATGATGGCAAGGGTGATAGG	SYBR
D loop (short)	F: TGACTATCCCCTTCCCCATT R: TTGTTGGTTTCACGGAGGAT	SYBR Green
COII/ATPase 6 (short)	F: TCTCCCCTCTCTACGCATTC R: CGGTTAATACGGGGTTGTTG	SYBR Green
ND5 (short)	F: GGCCTCACATCATCACTCCT R: GCTGTGGATCCGTTCGTAGT	SYBR Green

ND2/ND1 (short)	F: GGATGAGCCTCAAACTCCAA R: GGCTCGTAAAGCTCCGAATA	SYBR Green
ACTINB	Mm00607939_s1	TaqMan

Human

Target	Sequence	Platform
HK-2	Hs00606086_m1	TaqMan
GLUT1	Hs00892681_m1	TaqMan
IL-1α	Hs00174092_m1	TaqMan
IL-1β	Hs01555410_m1	TaqMan
TNFα	Hs00174128_m1	TaqMan
IL-6	Hs00174131_m1	TaqMan
IL-10	Hs00961622_m1	TaqMan
MT-ATP-6	Hs02596862_g1	TaqMan
MT-CO2	Hs02596865_g1	TaqMan
ND1	F: CCATAAAACCCGCCACACT R: GAGCGATGGTGAGAGCTAAGGT	SYBR
18S	F: CGCAGCTAGGAATAATGGAATAGG R: CATGGCCTCAGTTCCGAAA	SYBR
CNX43	Hs.PT.58.38338544	SYBR
COX2	Hs.PT.58.77266	SYBR
ACTB	Hs.PT.39a.22214847	SYBR
YWHAZ	Hs01122445_g1	TaqMan

Immunoblots. Antibodies are listed in Supplementary Table 2.

Supplementary Table 2.

Antibody	Species	Concentration	Source
CoxIV	Mouse IgG mAb	1:1,000	Cell Signaling Technology, #11967S

α-mouse-HRP conjugate	Rabbit IgG mAb	1:10,000	Cell Signaling Technology, # 58802S
β-Actin-HRP conjugate	Rabbit IgG mAb	1:2,000	Cell Signaling Technology, # 5125S
HIF1	Rabbit	1:1000	Cell Signaling Technology,

SA-β-Galactosidase Assay. Adherent cells were fixed and stained for SA-βGal via a Senescence Detection kit (Abcam, ab65351) per manufacturer's instructions. Cells with strong blue stain were considered positive for SA β-Gal stain. Representative images were used to calculate a fraction of SA-β-Gal-positive cells, scored by an observer blinded to treatment condition.

Live cell staining. Adherent cells were stained using the TMRE-Mitochondrial Membrane Potential Assay Kit (Abcam, ab113852) per manufacturer's instructions. Select wells were pretreated with 20 µM FCCP, a decoupling agent, as a positive control for 20 minutes before TMRE and Hoechst counterstain was applied. Live JAR cells were analyzed by the Celigo Image Cytometer (Nexcelom BioScience) for fluorescence quantification and gating. Adherent live JAR cells were also stained with MitoSOX™ Red Mitochondrial Superoxide Indicator kit (Invitrogen) and analyzed using the cytometer in a similar manner.

Cell counting. JAR cells were cultured for 6 days ± cobalt chloride exposure prior to cell counting. On day 6 of cobalt chloride exposure, cells from each condition were replated in a 96-well plate in $CoCl_2$-free media at a density of 5 x 10^3 cells per well. Celigo Imaging Cytometer was used for automated cell counting (total cells per well) at 24-hour intervals.

Bulk RNA Sequencing, Geneset Enrichment Analysis, Weighted Gene Correlation Network Analysis

Full methods provided upon publication.

Statistics.

Student's two-tailed unpaired t-test, ordinary one-way, and two-way ANOVA statistical tests were applied as indicated to compare biological replicates in each experiment.

Acknowledgements:

We thank Dr. Jennifer Condon of Wayne State University School of Medicine for generously providing the hTERT-HM cell line.

Figure annotations were created with Biorender.com

Research reported in this publication was supported by the Institute of General Medical Sciences of the National Institutes of Health under award GM007592-41 (EJC).

References

1. Liu L, Oza S, Hogan D, Perin J, Rudan I, Lawn JE, et al. Global, regional, and national causes of child mortality in 2000-13, with projections to inform post-2015 priorities: an updated systematic analysis. *Lancet.* 2015;385(9966):430-40.
2. Blencowe H, Cousens S, Chou D, Oestergaard M, Say L, Moller AB, et al. Born too soon: the global epidemiology of 15 million preterm births. *Reprod Health.* 2013;10 Suppl 1:S2.
3. Goldenberg RL, Culhane JF, Iams JD, and Romero R. Epidemiology and causes of preterm birth. *Lancet.* 2008;371(9606):75-84.
4. Smith V, Devane D, Begley CM, Clarke M, and Higgins S. A systematic review and quality assessment of systematic reviews of randomised trials of interventions for preventing and treating preterm birth. *Eur J Obstet Gynecol Reprod Biol.* 2009;142(1):3-11.
5. Kiserud T, Ebbing C, Kessler J, and Rasmussen S. Fetal cardiac output, distribution to the placenta and impact of placental compromise. *Ultrasound Obstet Gynecol.* 2006;28(2):126-36.
6. Shaut CA, Keene DR, Sorensen LK, Li DY, and Stadler HS. HOXA13 Is essential for placental vascular patterning and labyrinth endothelial specification. *PLoS Genet.* 2008;4(5):e1000073.
7. Lykke JA, Langhoff-Roos J, Sibai BM, Funai EF, Triche EW, and Paidas MJ. Hypertensive pregnancy disorders and subsequent cardiovascular morbidity and type 2 diabetes mellitus in the mother. *Hypertension.* 2009;53(6):944-51.
8. Genbacev O, Joslin R, Damsky CH, Polliotti BM, and Fisher SJ. Hypoxia alters early gestation human cytotrophoblast differentiation/invasion in vitro and models the placental defects that occur in preeclampsia. *J Clin Invest.* 1996;97(2):540-50.
9. Plaks V, Rinkenberger J, Dai J, Flannery M, Sund M, Kanasaki K, et al. Matrix metalloproteinase-9 deficiency phenocopies features of preeclampsia and intrauterine growth restriction. *Proc Natl Acad Sci U S A.* 2013;110(27):11109-14.

10. Li F, Fushima T, Oyanagi G, Townley-Tilson HW, Sato E, Nakada H, et al. Nicotinamide benefits both mothers and pups in two contrasting mouse models of preeclampsia. *Proc Natl Acad Sci U S A.* 2016;113(47):13450-5.
11. Romero R, and Chaiworapongsa T. Preeclampsia: a link between trophoblast dysregulation and an antiangiogenic state. *J Clin Invest.* 2013;123(7):2775-7.
12. McIntyre KR, Vincent KMM, Hayward CE, Li X, Sibley CP, Desforges M, et al. Human placental uptake of glutamine and glutamate is reduced in fetal growth restriction. *Sci Rep.* 2020;10(1):16197.
13. Xu YY, Liu Y, Cui L, Wu WB, Quinn MJ, Menon R, et al. Hypoxic effects on the mitochondrial content and functions of the placenta in fetal growth restriction. *Placenta.* 2021;114:100-7.
14. Koga K, Cardenas I, Aldo P, Abrahams VM, Peng B, Fill S, et al. Activation of TLR3 in the trophoblast is associated with preterm delivery. *Am J Reprod Immunol.* 2009;61(3):196-212.
15. Pique-Regi R, Romero R, Tarca AL, Sendler ED, Xu Y, Garcia-Flores V, et al. Single cell transcriptional signatures of the human placenta in term and preterm parturition. *Elife.* 2019;8.
16. Beharier O, Tyurin VA, Goff JP, Guerrero-Santoro J, Kajiwara K, Chu T, et al. PLA2G6 guards placental trophoblasts against ferroptotic injury. *Proc Natl Acad Sci U S A.* 2020;117(44):27319-28.
17. Elshenawy S, Pinney SE, Stuart T, Doulias PT, Zura G, Parry S, et al. The Metabolomic Signature of the Placenta in Spontaneous Preterm Birth. *Int J Mol Sci.* 2020;21(3).
18. Lien YC, Zhang Z, Cheng Y, Polyak E, Sillers L, Falk MJ, et al. Human Placental Transcriptome Reveals Critical Alterations in Inflammation and Energy Metabolism with Fetal Sex Differences in Spontaneous Preterm Birth. *Int J Mol Sci.* 2021;22(15).
19. Paquette AG, Brockway HM, Price ND, and Muglia LJ. Comparative transcriptomic analysis of human placentae at term and preterm delivery. *Biol Reprod.* 2018;98(1):89-101.
20. Knox K, and Baker JC. Genomic evolution of the placenta using co-option and duplication and divergence. *Genome Res.* 2008;18(5):695-705.
21. Zhou QY, Fang MD, Huang TH, Li CC, Yu M, and Zhao SH. Detection of differentially expressed genes between Erhualian and Large White placentas on day 75 and 90 of gestation. *BMC Genomics.* 2009;10:337.
22. Loux SC, Dini P, El-Sheikh Ali H, Kalbfleisch T, and Ball BA. Characterization of the placental transcriptome through mid to late gestation in the mare. *PLoS One.* 2019;14(11):e0224497.
23. Soncin F, Khater M, To C, Pizzo D, Farah O, Wakeland A, et al. Comparative analysis of mouse and human placentae across gestation reveals species-specific regulators of placental development. *Development.* 2018;145(2).
24. Maeda KJ, Showmaker KC, Johnson AC, Garrett MR, and Sasser JM. Spontaneous superimposed preeclampsia: chronology and expression unveiled by temporal transcriptomic analysis. *Physiol Genomics.* 2019;51(8):342-55.

25. Morey R, Farah O, Kallol S, Requena DF, Meads M, Moretto-Zita M, et al. Transcriptomic Drivers of Differentiation, Maturation, and Polyploidy in Human Extravillous Trophoblast. *Front Cell Dev Biol.* 2021;9:702046.
26. Steinhauser CB, Lambo CA, Askelson K, Burns GW, Behura SK, Spencer TE, et al. Placental Transcriptome Adaptations to Maternal Nutrient Restriction in Sheep. *Int J Mol Sci.* 2021;22(14).
27. Jang JY, Blum A, Liu J, and Finkel T. The role of mitochondria in aging. *J Clin Invest.* 2018;128(9):3662-70.
28. Trifunovic A, Wredenberg A, Falkenberg M, Spelbrink JN, Rovio AT, Bruder CE, et al. Premature ageing in mice expressing defective mitochondrial DNA polymerase. *Nature.* 2004;429(6990):417-23.
29. Rothfuss O, Gasser T, and Patenge N. Analysis of differential DNA damage in the mitochondrial genome employing a semi-long run real-time PCR approach. *Nucleic Acids Res.* 2010;38(4):e24.
30. Bratic A, and Larsson NG. The role of mitochondria in aging. *J Clin Invest.* 2013;123(3):951-7.
31. Wiley CD, and Campisi J. From Ancient Pathways to Aging Cells-Connecting Metabolism and Cellular Senescence. *Cell Metab.* 2016;23(6):1013-21.
32. Wiley CD, and Campisi J. The metabolic roots of senescence: mechanisms and opportunities for intervention. *Nat Metab.* 2021;3(10):1290-301.
33. Nursalim YNS, Blenkiron C, Groom KM, and Chamley LW. Growing human trophoblasts in vitro: a review of the media commonly used in trophoblast cell culture. *Reproduction.* 2020;160(6):R119-R28.
34. Rothbauer M, Patel N, Gondola H, Siwetz M, Huppertz B, and Ertl P. A comparative study of five physiological key parameters between four different human trophoblast-derived cell lines. *Sci Rep.* 2017;7(1):5892.
35. Tong D, Lu X, Wang HX, Plante I, Lui E, Laird DW, et al. A dominant loss-of-function GJA1 (Cx43) mutant impairs parturition in the mouse. *Biol Reprod.* 2009;80(6):1099-106.
36. Nishimura F, Mogami H, Moriuchi K, Chigusa Y, Mandai M, and Kondoh E. Mechanisms of thrombin-Induced myometrial contractions: Potential targets of progesterone. *PLoS One.* 2020;15(5):e0231944.
37. Rauk PN, and Chiao JP. Interleukin-1 stimulates human uterine prostaglandin production through induction of cyclooxygenase-2 expression. *Am J Reprod Immunol.* 2000;43(3):152-9.
38. Leimert KB, Verstraeten BSE, Messer A, Nemati R, Blackadar K, Fang X, et al. Cooperative effects of sequential PGF2alpha and IL-1beta on IL-6 and COX-2 expression in human myometrial cellsdagger. *Biol Reprod.* 2019;100(5):1370-85.
39. Campisi J, Kapahi P, Lithgow GJ, Melov S, Newman JC, and Verdin E. From discoveries in ageing research to therapeutics for healthy ageing. *Nature.* 2019;571(7764):183-92.
40. Rosso P. Placenta as an aging organ. *Curr Concepts Nutr.* 1976;4:23-41.
41. Martin BJ, and Spicer SS. Ultrastructural features of cellular maturation and aging in human trophoblast. *J Ultrastruct Res.* 1973;43(1):133-49.
42. Fox H. Aging of the placenta. *Arch Dis Child Fetal Neonatal Ed.* 1997;77(3):F171-5.

43. Sultana Z, Maiti K, Aitken J, Morris J, Dedman L, and Smith R. Oxidative stress, placental ageing-related pathologies and adverse pregnancy outcomes. *Am J Reprod Immunol.* 2017;77(5).
44. Cindrova-Davies T, Fogarty NME, Jones CJP, Kingdom J, and Burton GJ. Evidence of oxidative stress-induced senescence in mature, post-mature and pathological human placentas. *Placenta.* 2018;68:15-22.
45. Biron-Shental T, Sukenik-Halevy R, Sharon Y, Goldberg-Bittman L, Kidron D, Fejgin MD, et al. Short telomeres may play a role in placental dysfunction in preeclampsia and intrauterine growth restriction. *Am J Obstet Gynecol.* 2010;202(4):381 e1-7.
46. Chen KH, Chen LR, and Lee YH. Exploring the relationship between preterm placental calcification and adverse maternal and fetal outcome. *Ultrasound Obstet Gynecol.* 2011;37(3):328-34.
47. Maiti K, Sultana Z, Aitken RJ, Morris J, Park F, Andrew B, et al. Evidence that fetal death is associated with placental aging. *Am J Obstet Gynecol.* 2017;217(4):441 e1- e14.
48. Bonney EA, Krebs K, Saade G, Kechichian T, Trivedi J, Huaizhi Y, et al. Differential senescence in feto-maternal tissues during mouse pregnancy. *Placenta.* 2016;43:26-34.
49. Menon R, Behnia F, Polettini J, Saade GR, Campisi J, and Velarde M. Placental membrane aging and HMGB1 signaling associated with human parturition. *Aging (Albany NY).* 2016;8(2):216-30.
50. Menon R, Richardson LS, and Lappas M. Fetal membrane architecture, aging and inflammation in pregnancy and parturition. *Placenta.* 2019;79:40-5.
51. Nye GA, Ingram E, Johnstone ED, Jensen OE, Schneider H, Lewis RM, et al. Human placental oxygenation in late gestation: experimental and theoretical approaches. *J Physiol.* 2018;596(23):5523-34.
52. Gomes AP, Price NL, Ling AJ, Moslehi JJ, Montgomery MK, Rajman L, et al. Declining NAD(+) induces a pseudohypoxic state disrupting nuclear-mitochondrial communication during aging. *Cell.* 2013;155(7):1624-38.
53. Gonzalez TL, Eisman LE, Joshi NV, Flowers AE, Wu D, Wang Y, et al. High-throughput miRNA sequencing of the human placenta: expression throughout gestation. *Epigenomics.* 2021;13(13):995-1012.
54. Sferruzzi-Perri AN, Higgins JS, Vaughan OR, Murray AJ, and Fowden AL. Placental mitochondria adapt developmentally and in response to hypoxia to support fetal growth. *Proc Natl Acad Sci U S A.* 2019;116(5):1621-6.
55. Rasmussen S, Ebbing C, and Irgens LM. Predicting preeclampsia from a history of preterm birth. *PLoS One.* 2017;12(7):e0181016.
56. Mando C, De Palma C, Stampalija T, Anelli GM, Figus M, Novielli C, et al. Placental mitochondrial content and function in intrauterine growth restriction and preeclampsia. *Am J Physiol Endocrinol Metab.* 2014;306(4):E404-13.
57. Fujimaki A, Watanabe K, Mori T, Kimura C, Shinohara K, and Wakatsuki A. Placental oxidative DNA damage and its repair in preeclamptic women with fetal growth restriction. *Placenta.* 2011;32(5):367-72.
58. Davy P, Nagata M, Bullard P, Fogelson NS, and Allsopp R. Fetal growth restriction is associated with accelerated telomere shortening and increased expression of cell senescence markers in the placenta. *Placenta.* 2009;30(6):539-42.

59. Burton GJ, Yung HW, Cindrova-Davies T, and Charnock-Jones DS. Placental endoplasmic reticulum stress and oxidative stress in the pathophysiology of unexplained intrauterine growth restriction and early onset preeclampsia. *Placenta.* 2009;30 Suppl A:S43-8.
60. Pennington KA, Schlitt JM, and Schulz LC. Isolation of primary mouse trophoblast cells and trophoblast invasion assay. *J Vis Exp.* 2012(59):e3202.

A

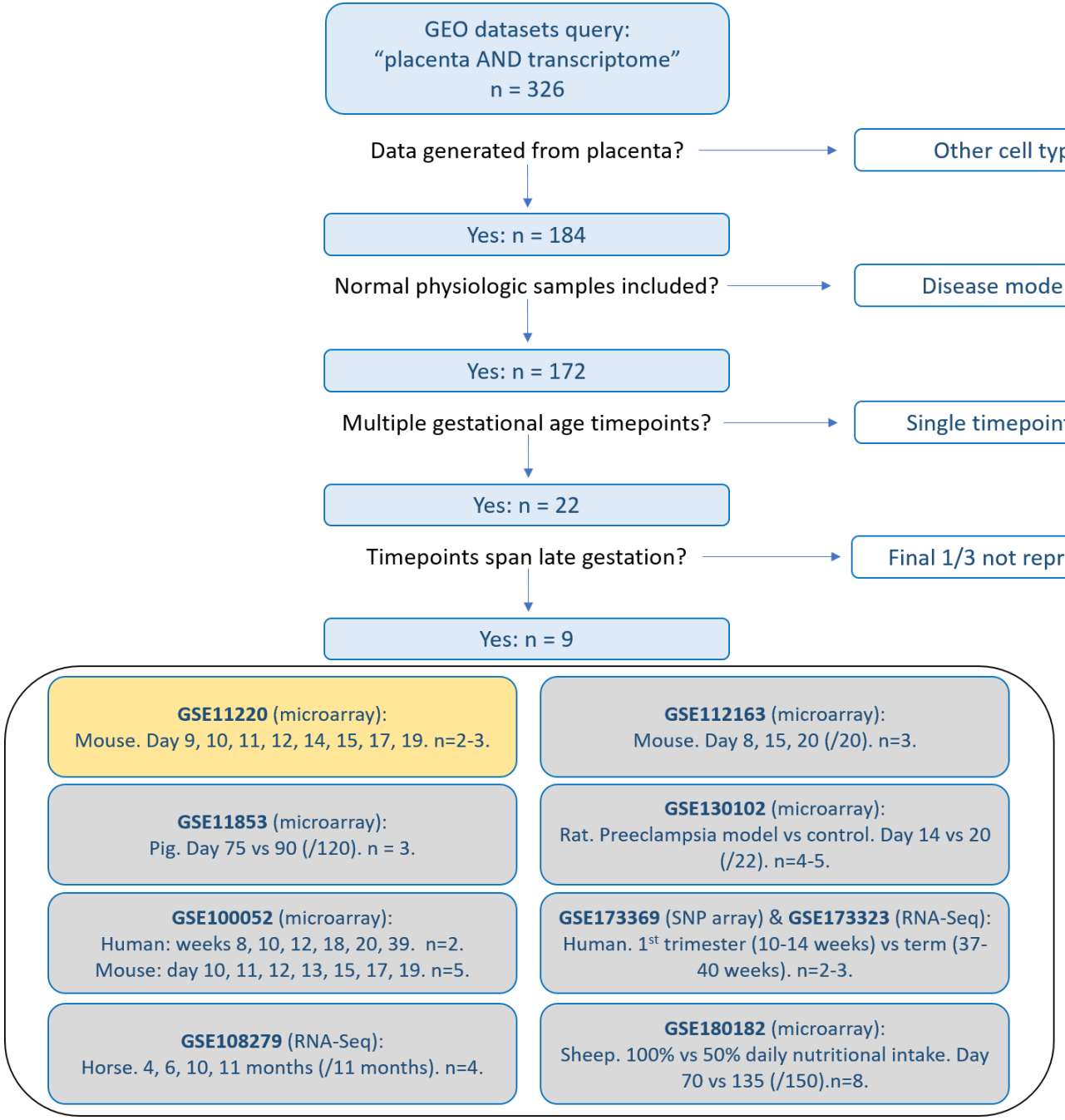
GEO datasets query:
"placenta AND transcriptome"
n = 326
Data generated from placenta?
Other cell types: n = 142
Yes: n = 184
Normal physiologic samples included?
Disease model only: n = 12
Yes: n = 172
Multiple gestational age timepoints?
Single timepoint only: n = 150
Yes: n = 22
Timepoints span late gestation?
Final 1/3 not represented: n = 13
Yes: n = 9
GSE11220 (microarray):
Mouse. Day 9, 10, 11, 12, 14, 15, 17, 19. n=2-3.
GSE112163 (microarray):
Mouse. Day 8, 15, 20 (/20). n=3.
GSE11853 (microarray):
Pig. Day 75 vs 90 (/120). n = 3.
GSE130102 (microarray):
Rat. Preeclampsia model vs control. Day 14 vs 20 (/22). n=4-5.
GSE100052 (microarray):
Human: weeks 8, 10, 12, 18, 20, 39. n=2.
Mouse: day 10, 11, 12, 13, 15, 17, 19. n=5.
GSE173369 (SNP array) & GSE173323 (RNA-Seq):
Human. 1st trimester (10-14 weeks) vs term (37-40 weeks). n=2-3.
GSE108279 (RNA-Seq):
Horse. 4, 6, 10, 11 months (/11 months). n=4.
GSE180182 (microarray):
Sheep. 100% vs 50% daily nutritional intake. Day 70 vs 135 (/150).n=8.

Figure 1

Figure 1

B

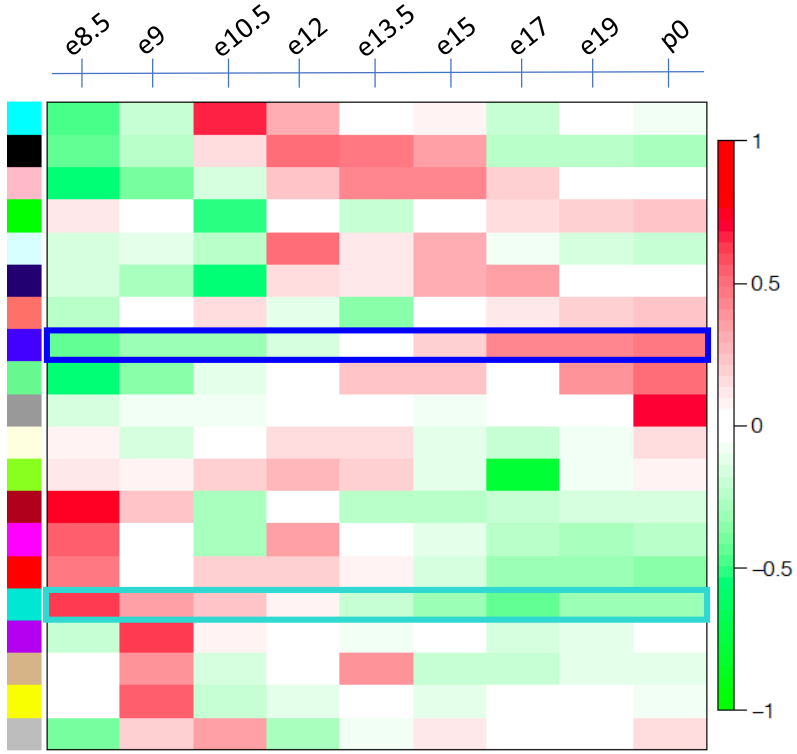

Term name	p_{adj}	$-\log_{10}(p_{adj})$ (0 – ≤16)
FoxO signaling pathway	1.540×10^{-6}	
Mitophagy - animal	4.698×10^{-6}	
mTOR signaling pathway	1.421×10^{-4}	
Cellular senescence	2.320×10^{-3}	
AMPK signaling pathway	1.856×10^{-2}	
HIF-1 signaling pathway	2.270×10^{-2}	

blue

Term name	p_{adj}	$-\log_{10}(p_{adj})$ (0 – ≤16)
Cell Cycle, Mitotic	1.028×10^{-31}	
Mitochondrial translation	9.363×10^{-20}	
Complex I biogenesis	7.630×10^{-7}	
Respiratory electron transport	9.573×10^{-6}	
Citric acid cycle (TCA cycle)	2.281×10^{-3}	

turquoise

C

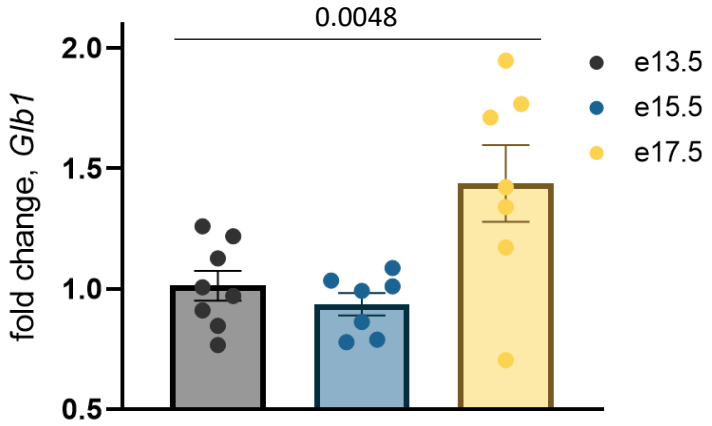

D

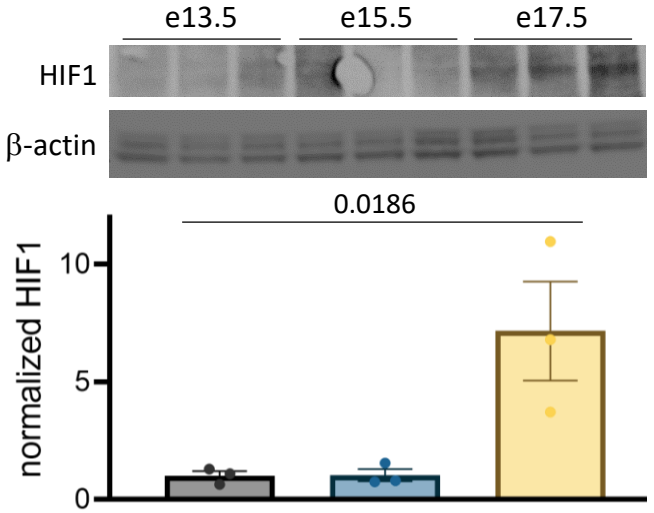

E

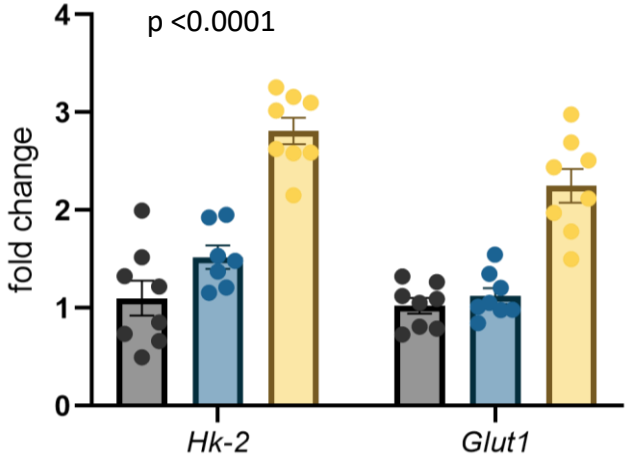

Figure 1

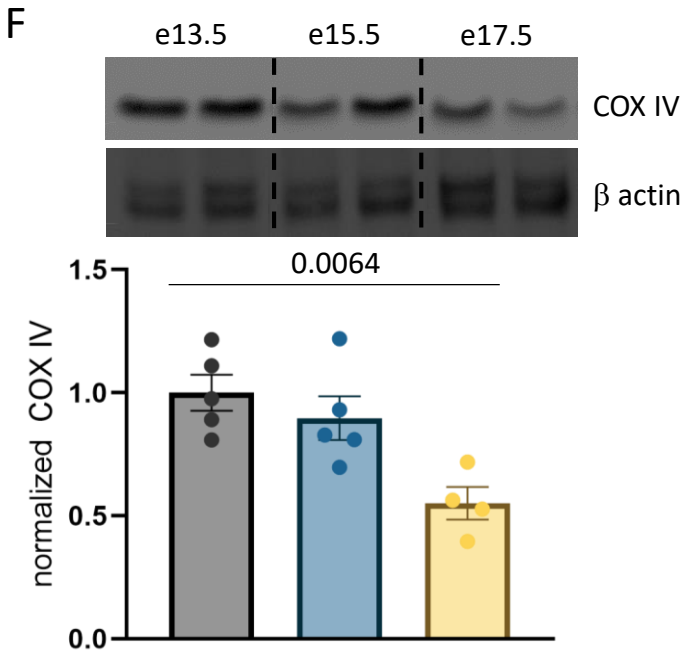
F
e13.5
e15.5
e17.5
COX IV
β actin
0.0064
normalized COX IV
1.5
1.0
0.5
0.0

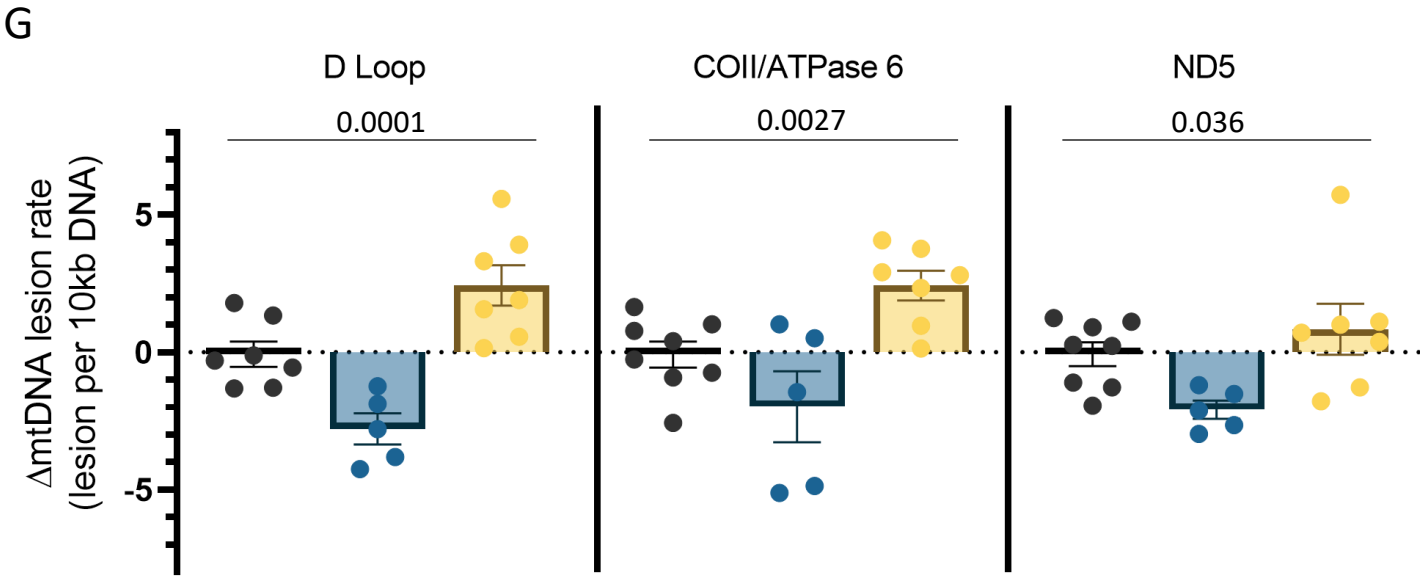
G
D Loop
COII/ATPase 6
ND5
0.0001
0.0027
0.036
ΔmtDNA lesion rate
(lesion per 10kb DNA)
5
0
-5

Table 1. Maternal and fetal characteristics

	< 35 weeks	> 39 weeks	p value
	n = 8	n = 10	
gestational age at delivery (weeks)	34.2 +/- 0.92	39.6 +/- 0.3	< 0.0001
maternal age (years)	32.5 +/- 1.8	36.5 +/- 3.1	0.006
maternal BMI > 40	1 (12.5)	0 (0)	0.25
maternal race			
White	6 (75)	8 (80)	0.13
Black	2 (25)	0 (0)	
Asian	0 (0)	2 (20)	
underlying maternal disease			
hypothyroidism	1 (12.5)	0 (0)	0.25
primiparous	3 (37.5)	3 (30)	0.73
female neonate	4 (50)	8 (80)	0.18
indication for delivery	placenta previa (3); vasa previa (3); thinned LUS (1); uterine dehiscience (1)	scheduled repeat (7); breech presentation (3)	

Figure 2

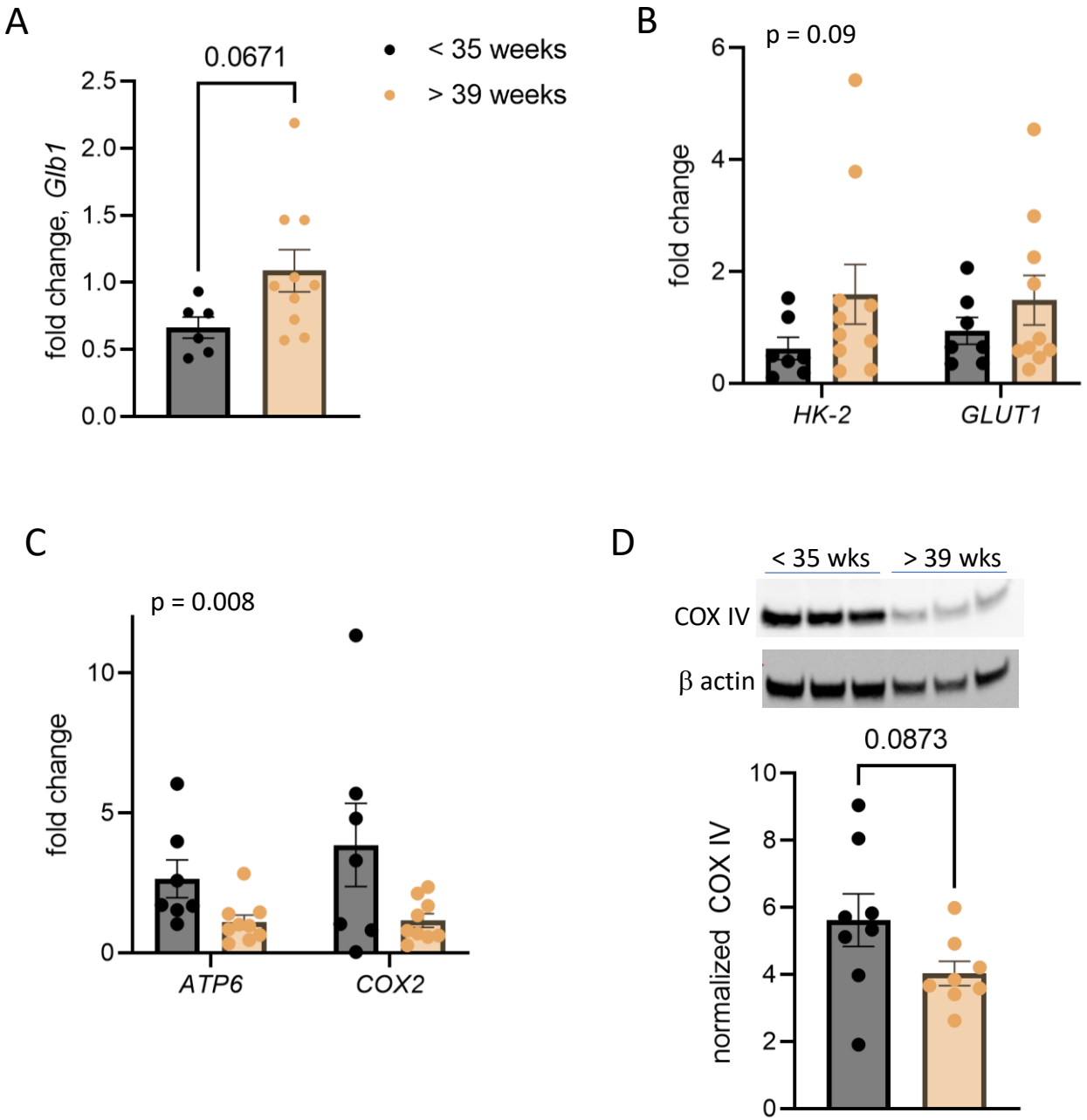
A
0.0671
< 35 weeks
> 39 weeks
fold change, Glb1
2.5
2.0
1.5
1.0
0.5
0.0
B
p = 0.09
fold change
6
4
2
0
HK-2
GLUT1
C
p = 0.008
fold change
10
5
0
ATP6
COX2
D
< 35 wks
> 39 wks
COX IV
β actin
0.0873
normalized COX IV
10
8
6
4
2
0

Figure 3

A

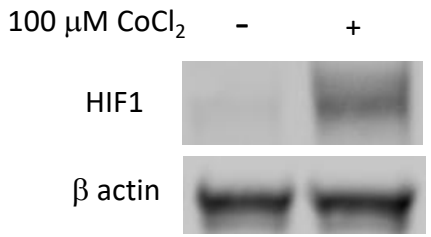

B

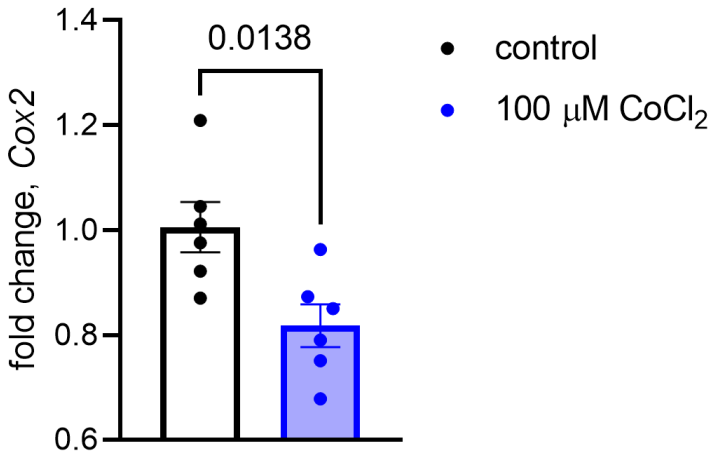

C

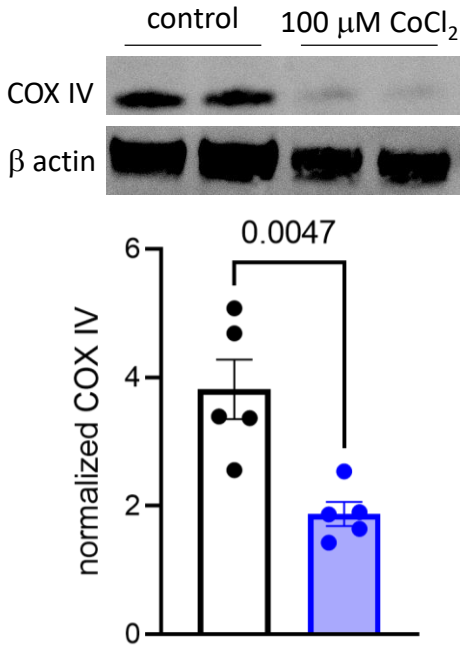

D

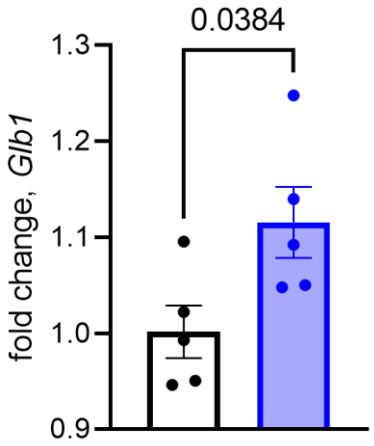

E

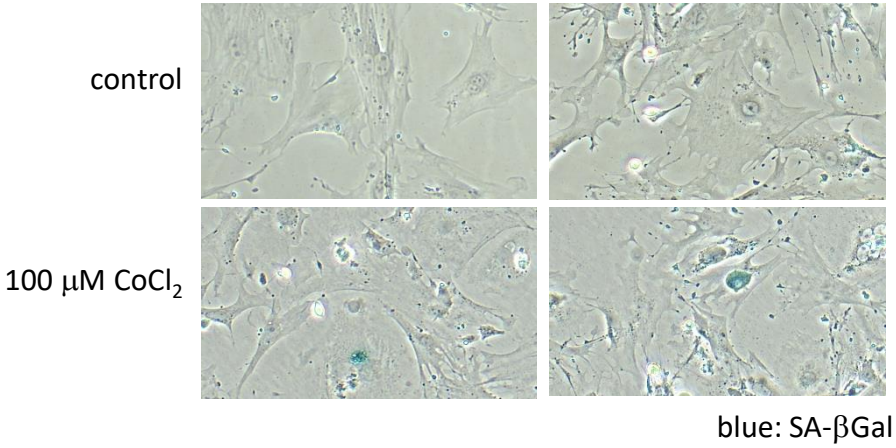

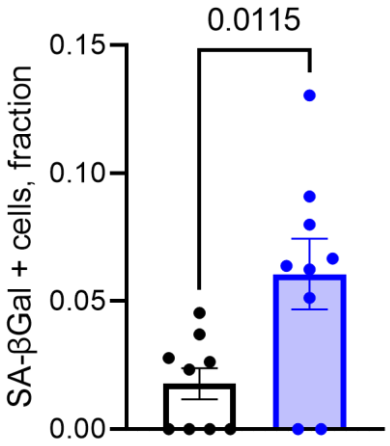

Figure 4

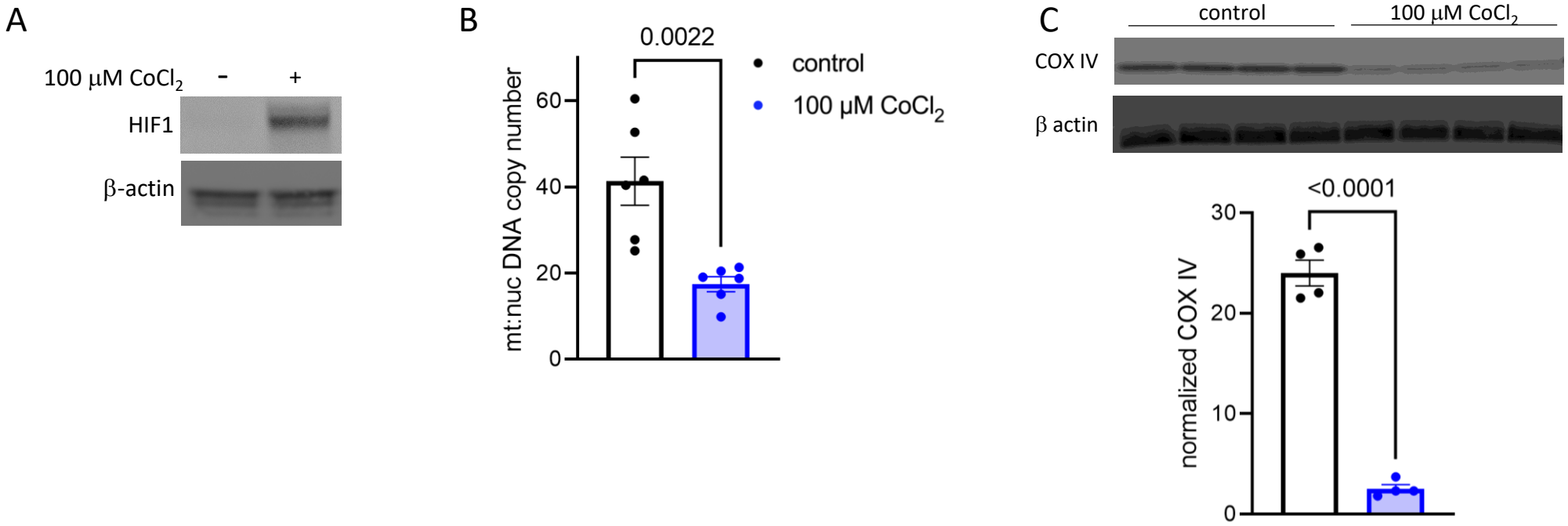
A
100 μM CoCl2
-
+
HIF1
β-actin
B
0.0022
control
100 μM CoCl2
mt:nuc DNA copy number
60
40
20
0
C
control
100 μM CoCl2
COX IV
β actin
<0.0001
normalized COX IV
30
20
10
0

Figure 4

D

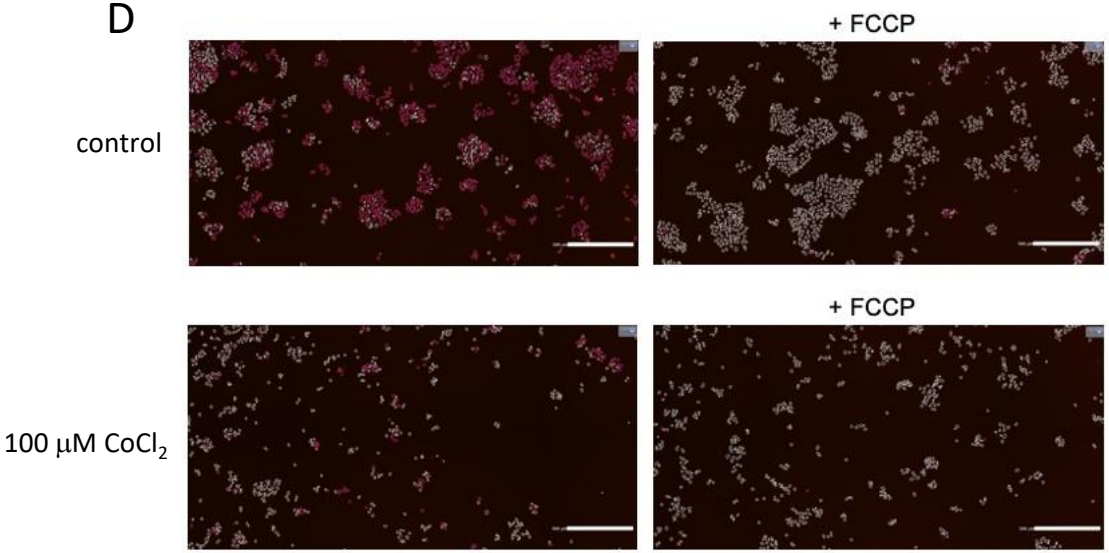

Pink = high TMRE; White = low TMRE

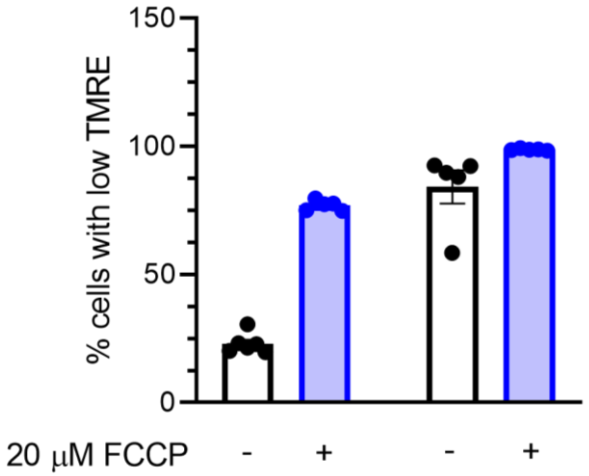

E

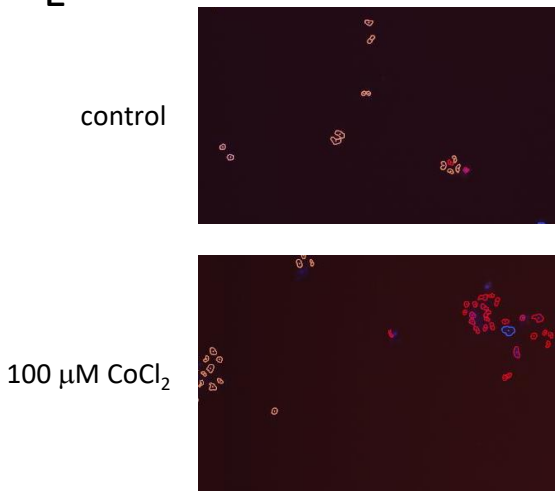

Red = high MtSox

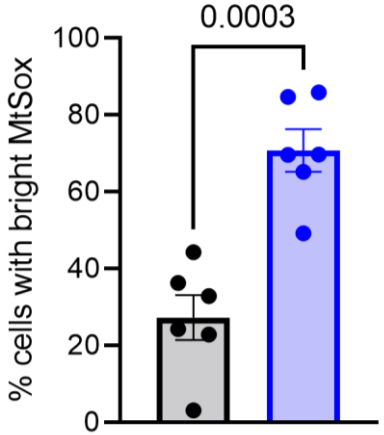

Figure 4

F

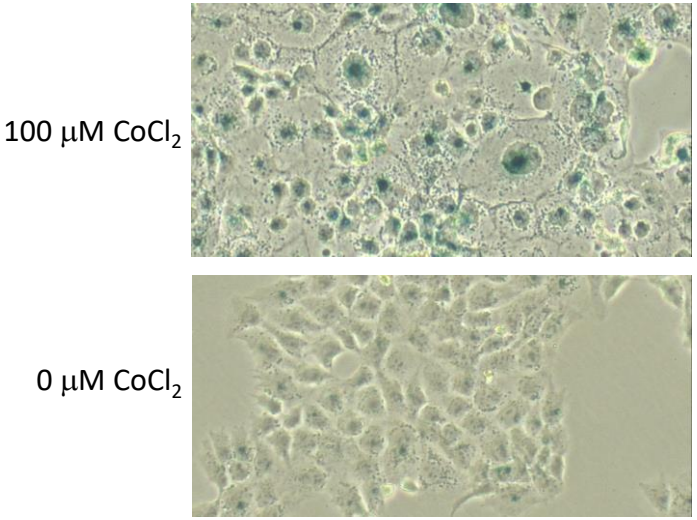

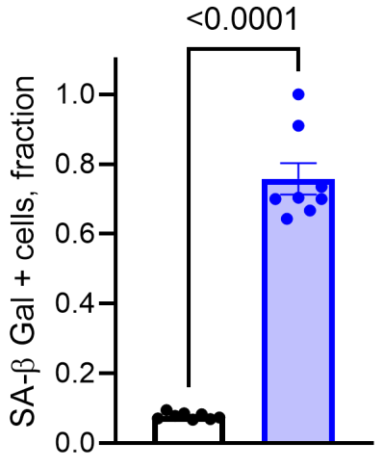

G

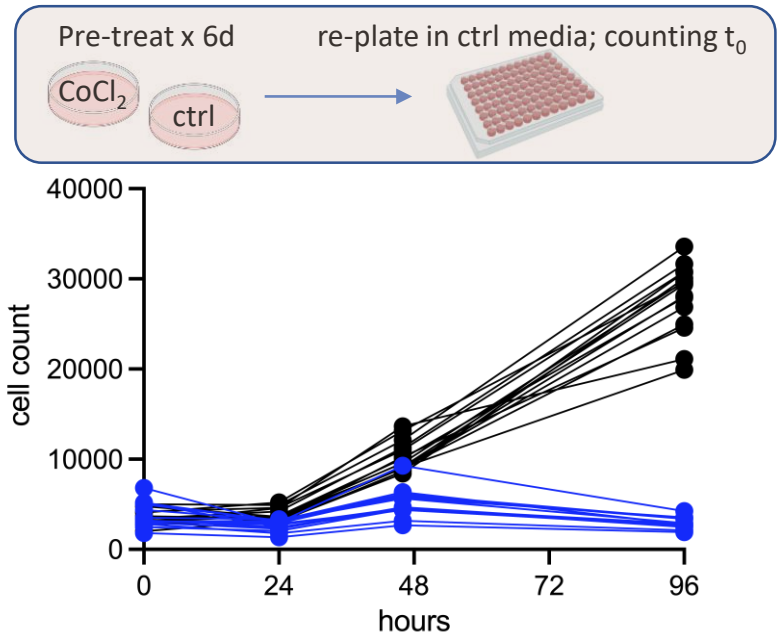

H

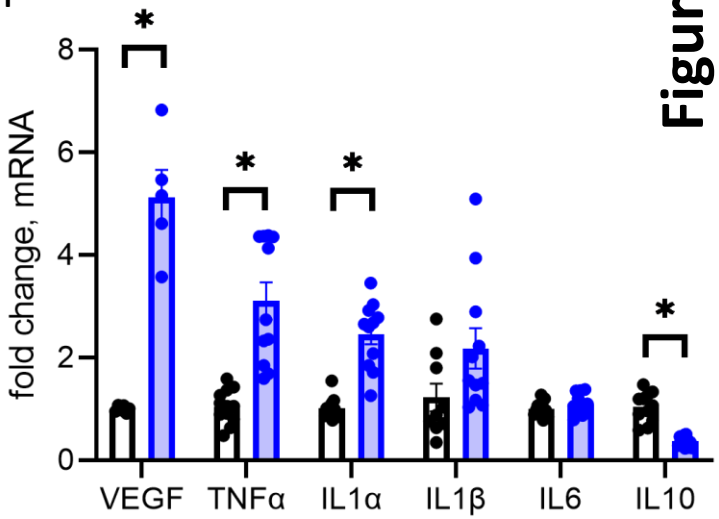

I

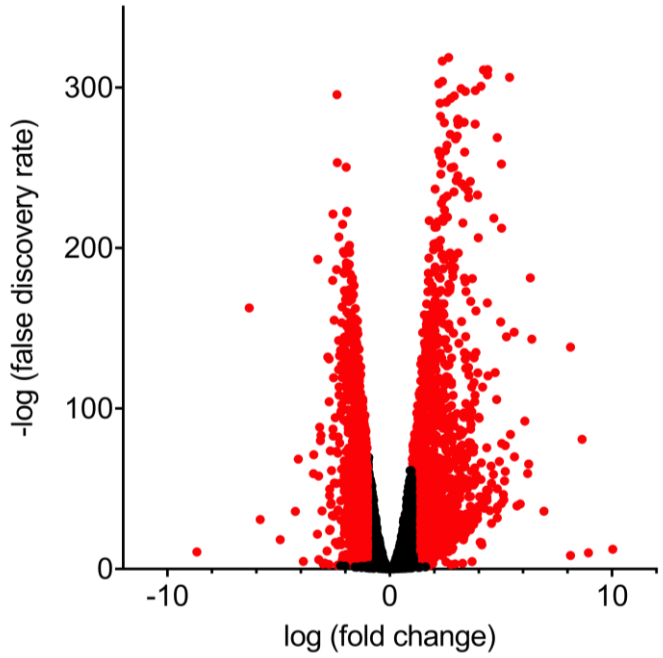

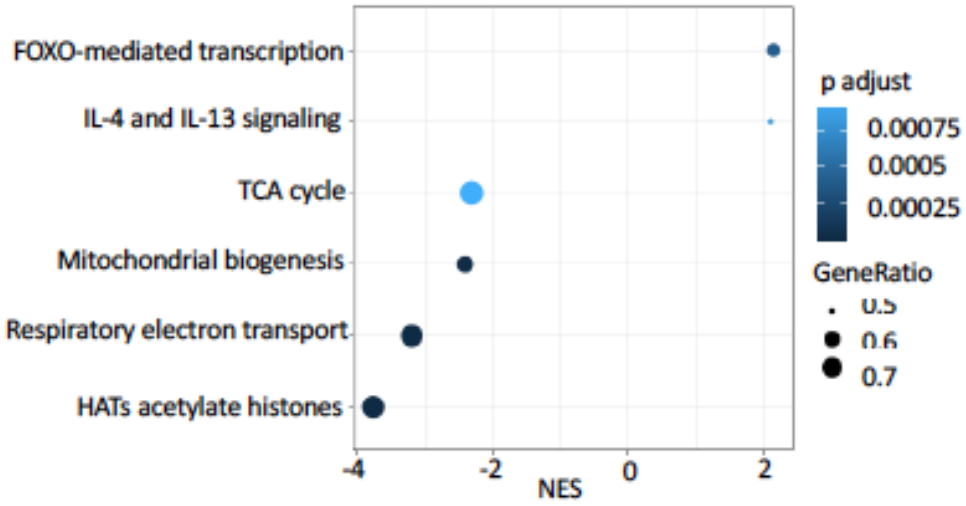

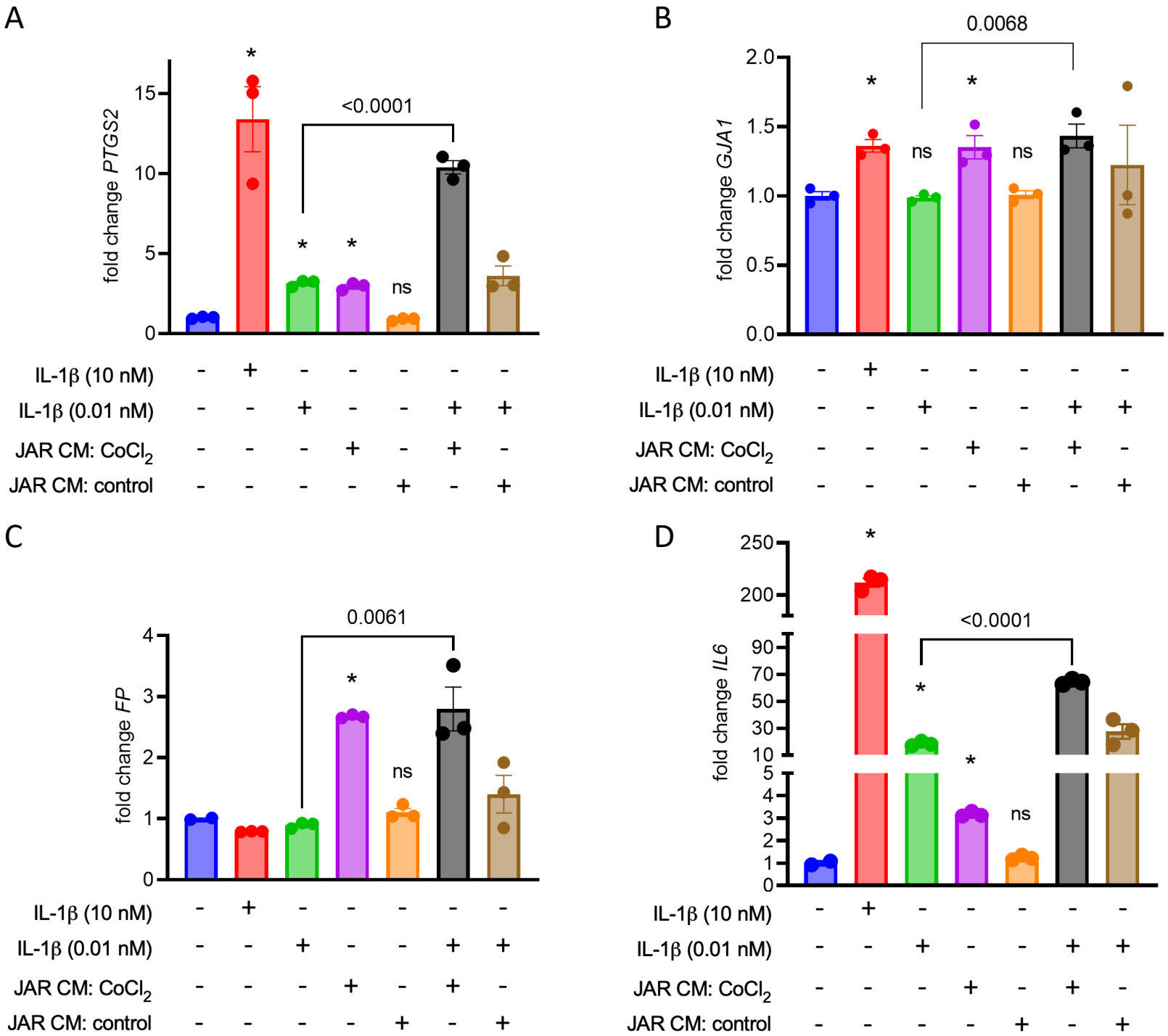
A
fold change PTGS2
15
10
5
0
*
<0.0001
*
*
ns
IL-1β (10 nM) - + - - - - -
IL-1β (0.01 nM) - - + - - + +
JAR CM: CoCl2 - - - + - + -
JAR CM: control - - - - + - +
B
fold change GJA1
2.0
1.5
1.0
0.5
0.0
0.0068
*
*
ns
ns
IL-1β (10 nM) - + - - - - -
IL-1β (0.01 nM) - - + - - + +
JAR CM: CoCl2 - - - + - + -
JAR CM: control - - - - + - +
C
fold change FP
4
3
2
1
0
0.0061
*
ns
IL-1β (10 nM) - + - - - - -
IL-1β (0.01 nM) - - + - - + +
JAR CM: CoCl2 - - - + - + -
JAR CM: control - - - - + - +
D
fold change IL6
250
200
90
70
50
30
10
5
4
3
2
1
0
*
<0.0001
*
*
ns
IL-1β (10 nM) - + - - - - -
IL-1β (0.01 nM) - - + - - + +
JAR CM: CoCl2 - - - + - + -
JAR CM: control - - - - + - +

Figure 5